PCCP

Cage-like effect in Au-Pt nanoparticle synthesis in microemulsions: A simulation study

Journal:	*Physical Chemistry Chemical Physics*
Manuscript ID:	CP-ART-07-2014-002936.R1
Article Type:	Paper
Date Submitted by the Author:	04-Aug-2014

Complete List of Authors:	Tojo, Concha; University of Vigo, Physical Chemistry De Dios, Miguel; University of Vigo, Applied Physics Buceta, David; University of Santiago de Compostela, Physical Chemistry Department Lopez-Quintela, M.A. ; University of Santiago de Compostela, Physical Chemistry Department

Journal Name

RSCPublishing

ARTICLE

Cage-like effect in Au-Pt nanoparticle synthesis in microemulsions: A simulation study

Cite this: DOI: 10.1039/x0xx00000x

C. Tojo,[a] M. de Dios,[a] D. Buceta[b] and M. A. López-Quintela[b]

Received ooth January 2012,
Accepted ooth January 2012

DOI: 10.1039/x0xx00000x

www.rsc.org/

The different distributions of metals in bimetallic nanoparticles synthesized in microemulsion were studied by computer simulation. The simulations demonstrated that if the difference between the reduction potentials of both metals is about 0,15-0,3 V, the compartmentalization of the reaction media causes the accumulation of slower reduction reactants in the microemulsions droplets, which favours the chemical reaction like a cage effect: increasing the local concentration of the slower reduction metal salt gives rise to a faster reduction, so the differences in reduction rates of both metals are attenuated. A more coincidental reduction of both metals deeply affects the nanoparticle structure, causing a better mixed alloy. This effect will be more pronounced when the concentration is higher and the intermicellar exchange rate is faster. This means that for any fixed microemulsion the nanoparticle structure can be modified by changing the reactant concentration: the core can be enriched in the faster reduction metal by lower concentrations, and the shell can be enriched in the slower metal by higher concentrations. Based on these observations, this study suggests a route to help experimentalists better create pre-defined structure nanoparticles.

1. Introduction

The use of nanostructures in catalytic processes is contributing to the development of new improved catalysts.[1,2] Of special importance are catalysts composed by two different metallic elements, since they are a field of scientific and technological interest. The importance of bimetallic nanoparticles in catalysis is due to the interplay between two different metals which composed the particle. This synergic interaction improves catalytic activity and selectivity, which are different from that of the corresponding monometallic nanoparticles.[3] Specifically, the arrangement of metals within the first few atomic layers from the surface determines the reaction efficiency and selectivity. In particular, the Au/Pt bimetallic nanoparticles have been extensively studied due to their high catalytic efficiency.[4,5] The improvement of the Au/Pt nanoparticles catalytic activity is explained by assuming that the gold core attracts electron from platinum, giving rise to a nanoparticle whose Pt shell is electron-deficient.[3] The catalytic activity of the Au/Pt bimetallic nanoparticles depends on its average size, electronic structure and composition,[5-7] as well as the preparation method.[6,8,9] Moreover, the importance of the bimetallic spatial distribution was recently showed for core-shell Au/Pt and Fe_3O_4/Au/Pt nanoparticles in electrocatalytic oxygen reduction and methanol oxidation reaction.[10] Likewise, the Pt nanoparticles modified with Au clusters has also been demonstrated to enhance catalyst stability against dissolution in the electrocatalytic oxygen reduction.[11] Recently a direct interdependence between the surface composition of Au/Pt particles and their catalytic activity has been established.[12] So the ability to control composition distribution of Au/Pt bimetallic nanoparticles is decisive in researching catalytic activity.

Although different novel approaches have been used for the synthesis of nanoparticles,[3-6,13-21] the precise control of the bimetallic nanostructures is still a challenge.[22,23] An alternative method to control the metal distribution and sizes of bimetallic nanoparticles is the microemulsion route.[9,24-26] In this method, small amounts of water are added to a mixture of surfactant and oil. The result is a water-in-oil microemulsion composed of nanometer-sized water droplet dispersed in an oil phase stabilized by the surfactant bilayer. The reactants (metal precursors and reducing agent) are solubilized inside the dispersed waterpools of two microemulsions. After mixing both microemulsions the formation of metal particles inside these aqueous nanoreactors can take place. A necessary step prior to chemical reaction is to transfer reagents to the same droplet, which is assumed to occur by direct material transference between colliding micelles. The main advantages of the microemulsion route are that it allows a better control over the size of bimetallic nanoparticles and it does not require high temperatures. However, changing the bimetallic distribution is a very difficult task even when microemulsions are used. Nowadays, the preparation of different nanostructures is only made possible by changing the microemulsion composition (different surfactant, cosurfactant, etc). This gives rise to nanostructured particles with different cappings, which complicates the comparison of their properties. It would be a great advance if the nanostructure could be modified just by changing a single parameter (such as concentration) using a

particular microemulsion. For this purpose and in order to adjust the conditions for synthesizing Au/Pt nanoparticles with specific nanostructures, we have carried out a Monte Carlo simulation study to determine whether the bimetallic nanoparticle structure could be modified just by changing only the reactants concentration. Recently Au/Pt nanoparticles were synthetized using the same conditions of the simulation studies. The amazing agreement between theoretical and experimental STEM profiles confirms the validity of the proposed model.[27] Therefore, the simulation procedure can be used not only as a tool to find new ways of synthesizing bimetallic nanoparticles with *ad-hoc* controlled nanostructures, but also as a means to further our understanding of the complex mechanisms governing the reactions in microemulsions. In fact one of the aims of our study has been to investigate why/how the interplay between the compartmentalization of reaction media and reactant concentration can induce changes in the sequence of metal deposition in the case of a moderate difference in reduction rates.

Previous simulation results showed that the arrangement of metal components in a bimetallic nanoparticle depends on the difference in chemical reduction rates[23,28] and in nucleation rates[29,30] of both metals, and that this distribution can be modified by a change in microemulsion composition. In the present work, a particular bimetallic system is studied, Au-Pt bimetallic nanoparticle. That is, chemical reduction rates and nucleation rates are kept constant, and the influence of reactant concentration and microemulsion composition on metals distribution in the nanoparticle is analyzed from a mechanistic point of view. In the synthesis of bimetallic nanoparticles, the nucleus develops to a particle by building up new layers, so that the order of deposition of the metals defines the resulting structure. It is assumed that when the synthesis takes place in a homogeneous media, the ions with a higher reduction potential are reduced first, so the difference in the reduction potential of two metal ions is the main factor determining the final structure of the particles: when the reduction potentials of both metal ions are very different a core-shell structure is obtained. On the contrary, an alloyed nanoparticle is obtained when the difference in reduction potential is small enough. This assumption was extended to synthesis in microemulsions, without taking into account the compartmentalization of the reaction media. Previous simulation studies allowed us to conclude that the nanoparticle structure is defined by the difference in the reduction rates only if both reductions occur at the same rate (an alloy is obtained) or if both reductions have very different rates (a core-shell structure is obtained).[28] These two extreme cases reproduce the behaviour obtained in homogeneous media, that is, compartmentalization of the reaction media cannot modify the metal arrangement. But a vast majority of bimetallic systems belong to the large interval between both extremes ($1 < v_A / v_B < 100$, being v_A and v_B the reduction rates of fast and slow metal respectively), in which the nanoparticle structure is strongly dependent on microemulsion composition.[28]

The present study is focused on the Au/Pt bimetallic system, whose structure was proven to be satisfactorily reproduced by simulation by means of a reduction rates ratio $v_{Au} / v_{Pt} = 10$.[27] The ratio between the reduction rates of the fast (v_A) and the slow (v_B) metal is a parameter used in the simulation model to characterize the nature of the metals. The value $v_A / v_B = 10$ can be associated to bimetallic couples whose difference in standard reduction potentials is $\Delta\varepsilon \approx 0.15$ - 0.3 V.[28] Therefore, our study can be generalized to other bimetallic nanoparticles whose $\Delta\varepsilon$ is within this range.

2. Model and simulation procedure

This model is based on a previous model, which was successfully applied to study different experimental results of various reactions in microemulsions.[31,32] The synthesis of Au/Pt bimetallic nanoparticles in microemulsions is believed to occur as follows: In the first place, the $AuCl_4^-$ ions located in a micelle are reduced giving rise to a Au core. Then the $PtCl_6^-$ ions located in the same micelle are reduced on the surface of the Au core. As a result, the difference in the rates of reduction of the Au and Pt ions leads to the formation of a core-shell structure.[24] Our algorithm simulates the kinetic course of the reaction as follows: The reactants are metal salts A^+ and B^+ ($AuCl_4^-$ and $PtCl_6^-$ ions to synthesize Au/Pt particles) and a reducing agent R (e.g. hydrazine) whose reduction produces a metallic atom (Au or Pt). Three separate identical microemulsions are prepared and each reactant is solubilised in one microemulsion. Then the three microemulsions are mixed together. Brownian motion of the microemulsions droplets leads to collision. It is assumed that the intermicellar exchange can only occur when a collision between two micelles is enough energetic to be able to establish a water channel between the micelles, forming a transient droplet dimmer. When micelles contains the metal salt (A^+ and/or B^+) and the reducing agent (R) undergo such fusion, irreversible chemical reduction can take place.

2.1 Microemulsion Description

The domain of the simulations used in this study is a single micelle. The microemulsion is simulated as a set of micelles, which are randomly placed on a three dimensional lattice. Micelles are allowed to perform random walks and collide with each other. The one-pot method is simulated as follows: equal volumes of three microemulsions, each one carrying one kind of reactant (the metal salt A^+, the metal salt B^+, and the reductor R), are mixed. Each simulation run starts with a different random distribution of these three sets of micelles. In this paper the fraction of volume occupied by micelles is a $\varphi = 10\%$.

2.2 Initial distribution of reactant molecules

The initial distribution of reactant species (metal salts A^+ and B^+, and reducing agent R) among the microemulsion droplets is assumed to be described by Poisson distribution. We present results using three different mean values of concentration: $\langle c_{A+} \rangle = \langle c_{B+} \rangle = 4$, 32, and 128 metal ions initially located in a droplet. These values were calculated to simulate concentrations 0.02 M, 0.16 M and 0.64 M, respectively (see reference 30 for details). The concentration of reductor was $\langle c_R \rangle = 2\langle c_{A+} \rangle$.

2.3 Motion, collision and time unit base

The diffusion of micelles is assumed to be governed by Brownian motion. The collisions are due to Brownian motion and only binary collisions are considered. When a collision is enough energetic, a water channel can be established between two colliding micelles. Droplets fuse to form a short-lived dimmer (fusion),[33] which allowed the exchange of material contents (reactants, products and/or growing particles). To save computation time all collision are assumed to be effective. That is, in each step, a 10% of micelles are randomly chosen to collide, fuse and redisperse, allowing material exchange. The composition of colliding micelles is modified after collision according to the criteria described below. Once micellar

composition is updated, one Monte Carlo step (mcs) is completed.

2.4 Intermicellar exchange protocol of reactants

When the same kind of reactant (metal salt or reducing agent) is carried by both colliding droplets, the criterion to define the redistribution of reactants between micelles is the concentration gradient: the reactant flow from the more to the less occupied droplet. The simulation parameter k_{ex} quantifies the maximum number of molecules of reactant (A^+, B^+ and/or R) which could be exchanged during a collision. That is, when the droplet with a higher occupation number carries a quantity of molecules greater than k_{ex}, a maximum number k_{ex} of reactant molecules can be transferred to the droplet containing less reactants. However, when the number of reactants to transfer is smaller than k_{ex} both colliding droplets will contain the same number of reactants after collision. The k_{ex} parameter governs the rate of reactants exchange. The interdroplet channel could be traversed with more or less difficulty depending on the particular characteristics of the each specie (charge, size, composition), so the interdroplet exchange parameter can also depend on material nature. However, the same value of k_{ex} for all reactants ($k_{ex,A^+} = k_{ex,B^+} = k_{ex,R} = k_{ex}$) is used in this investigation, because it is assumed that k_{ex} is mainly determined by microemulsion composition.[33-35]

2.5 Reduction rates

Collisions between two droplets containing different kind of reactants gives rise to redistribution of material between micelles, so molecules of one metal salt (A^+ or B^+) and the reductor (R) can be located inside the same micelle. At this stage, chemical reduction can take place inside the micelle. To consider different reactions rates, the percentage of reactants located in the same micelle which gives rise to products can be modified. An instantaneous reaction is simulated when v = 1, that is, 100% reactants inside the micelle give rise to products after a single collision. The influence of chemical reduction rate on the bimetallic nanoparticles formation can be studied by decreasing the value of v.

The reduction potentials of the two metal salts A^+ and B^+ are usually different, so both chemical reductions will occur at different rates. Therefore, two different v parameters are considered: v_A and v_B are the reduction rates of the metal salts A^+ ($A^+ + R \rightarrow A$) and B^+ ($B^+ + R \rightarrow B$), respectively. In all cases, the A metal is the quicker one, and its reduction rate is instantaneous (100% of A^+ inside the same droplet are reduced). The chemical reduction of the other metal salt is slow down: only 10% B^+ inside the micelle is reduced to B atoms, corresponding to the case $v_A / v_B = 10$. So B is the slower metal. When the three reactant molecules (A^+ and B^+ salts and reductor agent R) are located inside the same micelle at the same time, both reductions can take place. In this situation, the metal which is reduced at first is chosen at random. The rest of B metal salt and reducing agent remains in the micelle, and can be exchanged or can react in a posterior collision.

2.6 Nucleation

A nucleation event takes place when a small number of atoms (ions or molecules), which are free in solution, become arranged forming a thermodynamically stable cluster, upon which additional atoms are deposited as the cluster grows. Classical nucleation theory established that there is a critical nucleus size from which the nucleus can grow.[36] When nucleus is smaller than critical size, the cluster is spontaneously dissolved. The competition between the aggregate curvature (Laplace pressure) and the free energy favouring the growth of the new phase determines the value of the critical nucleus size. Likewise, the particular value of the critical nucleus size depends on composition. In microemulsions, nucleation requires the simultaneous presence inside the same micelle of enough atoms to exceed the critical nucleation number.[37,38] Nucleation is simulated by means of a parameter n_A^* (the critical nucleus size of metal A), which is compared with the actual amount of A metal atoms inside the same droplet: if it is smaller than n_A^*, A atoms remain free (non-aggregated) inside the droplet, so that they can be transferred during a posterior collision. The interchange of these free metal atoms is defined by the $k_{ex,P}$ parameter described below. However, if the A amount inside the micelle reaches the n_A^* value, all atoms come together giving rise to a stable nucleus capable of further growth. The exchange of nucleus between colliding micelles depends on the intermicellar channel size, because a nucleus have to be exchanged as a whole. This kind of material exchange is governed by the film flexibility parameter *f* (see below).

The simulation model distinguishes three different values of the critical nucleus size. On one hand, different metals require a different critical nucleus sizes, so two different values (n_A^* and n_B^*) can be considered. On the other hand, the possibility of a heterogeneous nucleation, that is, the aggregation of two different metals to form a nucleus, is also considered by the n_{AB}^* parameter. n_{AB}^* quantifies the minimum number of metal products (indistinctly A or B) within the same micelle required to form a heterogeneous nucleus capable of further growth. Because this parameter strongly affects nucleation rate[37,39,40] and bimetallic nanoparticle structure,[30] it was kept constant $n_A^* = n_B^* = n_{AB}^* = n^* = 1$ in order not to interfere in the discussion.

Alloying ability of bimetallic nanoparticles depends on the total Gibbs energy of an atomic assembly, which can vary with composition due to the different atomic binding energy of A-A, B-B, and A-B species. So the number of atoms required for the formation of a nucleus is dependent on composition. This phenomena is included in the simulation model by means of the three critical nucleus numbers (n_A^*, n_B^* and n_{A-B}^*). Once the critical number is exceed, the cluster grows by deposition of all metal atoms located inside the same micelle, so one nucleation event is assumed to occur in a micelle. The surface chemistry is not considered. Different atomic-scale simulations provide detailed information of the surface chemistry of bimetallic nanoparticles of different composition.[41,42]

2.7 Intermicellar exchange protocol of free metal products

As mentioned before, if the amount of metal atoms within a micelle is smaller than the critical nucleus size, atoms remain independent (no aggregated), so they can be exchanged between micelles in a posterior collision. This kind of intermicellar exchange is dictated by the metal product exchange parameter ($k_{ex,P}$), which quantifies the number of metal products (A and/or B atoms) which can be transferred in a collision. This parameter is closely related to the rate of intermicellar exchange of A/B metal atoms. The same k_{ex} for all free units (reactants and products) are used in this study ($k_{ex} = k_{ex,P}$). Whenever a metal atom is exchanged to a nucleated micelle, this atom is deposited on the nucleus, building up a growing particle P_i, being P the metallic products (A and/or B) and *i* the number of metal products.

It is important to note the physical significance of this exchange protocol. The k_{ex} parameter is related to microemulsion dynamics, specifically, it is closely related to the dimmer stability:[43] the more stable the dimmer the longer it remains together, and then more material can be exchanged during a collision. That is, if k_{ex} controls how many molecules can be exchanged in a collision, a high value of k_{ex} also implies that the micelles stay together for a longer time.

2.8 Growth by autocatalysis

Droplets can contain reactants and nuclei simultaneously as the synthesis advances. This situation allows to introduce the possibility of autocatalysis, by means of favouring chemical reduction in the presence of a growing nucleus as follows: if one of the colliding micelles is carrying a particle, the reduction takes place on that particle with double reaction rate. If both colliding micelles are nucleated, reaction proceeds in the micelle containing the larger particle.[23,28,44-45] In this way, the fact that a larger surface (a larger particle) has a greater probability to play as catalyst is taken into account. This exchange criterion is likely to produce a higher number of empty micelles, giving rise to less large particles, whose size distribution is narrower as experimentally observed.[45] Non-autocatalytic reactions were previously studied.[31] In this paper we present results considering autocatalytic reactions. This criterion only takes into account the particle size, independently of composition (A or B metals).

2.9 Intermicellar exchange protocol of particles

At later stages of the synthesis the exchange of particles (aggregates of metals) is more probable, because collisions between two nucleated micelles are frequent. The transfer of growing particle to another micelle containing a particle during the fusion process is allowed. Likewise, reactants, free metal atoms and growing particles are allowed to be exchanged during the same collision. With a bit of reflection, it can be assumed that intermicellar exchange of particles will be restricted by the size of the channel communicating colliding micelles, which is closely related to the surfactant film flexibility. In addition, the possibility of growth via ripening must be taken into account. Both phenomena are discussed as follows.

2.10 Growth by ripening

It is well known that solubilisation and condensation of material can modify particle size. A particular coarsening process is Ostwald ripening, which supposes that the easier solubilisation of the smallest particles causes their decreasing in size. This results in an increased amount of free atoms/ molecules in solution, which will deposit on the largest particles. That is, large particles grow even larger, drawing material from the smaller ones, which shrink. This possibility is included in the exchange protocol of particles as follows: a collision between a micelle containing a growing particle P_i, (being P the metallic atoms A and/or B, and i the number of metallic atoms) and another nucleated micelle P_j leads to the exchange of the smaller particle. This transfer is unidirectional, that is, smaller particle moves always from the initial micelle to the micelle containing the larger one ($P_i + P_j \rightarrow P_{i+j}$). This material intermicellar exchange will only take place if the channel size between micelles is large enough, that is, the channel size (see below) must be greater or equal to P_{i+j}. The particle composition (A or B metal) is not taken into consideration in this rule, which is only determined by the particle size.

2.11 Modelling material intermicellar exchange: channel size, dimmer stability and film flexibility

Material intermicellar exchange takes place during the dimmer formation, which implies the inversion of the surfactant film curvature. The flexibility of the film surrounding microemulsion droplets is defined as the ability of the film to leave the optimal curvature. Film rigidity is an important parameter associated with the interfacial curvature, which depends on the interactions at both sides of the interface. Surfactants can be classified as flexible or rigid, based on the strength of the interfacial interactions. In microemulsions, the surfactant must reduce the interfacial tension to a sufficiently low value, so that the free energy for creating new area of interface must be compensated for a large entropic contribution. That is, a surfactant will be enough flexible if it tolerates curvature fluctuations.[46,47] Therefore, the flexibility of the surfactant film surrounding micelles is directly related to the facility with which intermicellar channels can be established. On one hand, surfactant film flexibility restricts the size of the particles capable of crossing the interdroplet channels. As a result the more flexible the film, the larger particles can be exchanged. The surfactant film flexibility is introduced in the simulation model by means of the flexibility parameter (f), which specifies a maximum particle size for transfer between droplets: particles composed by more than f units (A and/or B metal atoms) are not allowed to be exchanged between micelles. This means that the f parameter is closely related to channel size:[48] a value $f = 30$ would correspond to a channel size of about 6-10 Å (30 metal atoms are aggregated in a spherical shape). Likewise, a channel size of around 1-2 Å is obtained for $f = 5$. On the other hand, material exchange between micelles will be possible not only if the size of the intermicellar channel is large enough, but also if micelles remain as a fused dimmer long enough. Therefore, a flexible film implies that a larger particle can be transferred (high f) and intermicellar exchange is faster (high k_{ex}).[43,48] This means that the flexibility f and the exchange rate k_{ex} parameters have to be closely related. The most important factor determining the interdroplet exchange of isolated atoms/molecules (reactants and free metals) is the dimmer stability. The intermicellar channel size would not be of interest in this case because free units traverse the intermicellar channel one by one. In contrast, the channel size is the main factor if the transferred material is an aggregate of atoms (a growing particle), whose exchange between micelles must take place as a whole. From this picture, the flexibility of the surfactant film is introduced in the model as follows: First, the k_{ex} parameter governs the exchange of free species (reactants and non-aggregated metallic atoms), which are exchanged one by one, and it is linked with the dimmer stability. Second, the f parameter restricts the size of a exchanged particle, and it is linked with the interdroplet channel size. Because both parameters have to rise together, to simulate a rigid, medium and flexible film, a channel size $f = 5$, 30 and 90 is associated with $k_{ex} = 1$, 5 and 15 free atoms to be transferred in a collision, respectively. Experimental results obtained in an AOT/n-heptane/water microemulsion was successful compared with simulation data when flexibility is characterized by $f = 5$ and $k_{ex} = 1$.[31]

2.12 Droplet size

Due to the surfactant film covering the droplet has a finite bending modulus, an important quantity of energy is needed to increase the droplet size. As a consequence, the nanoparticle growth may be restricted by the size of the droplets. The simulation includes a droplet size parameter, which limits the quantity of metal products which can be located inside the same droplet. In this study we present results using low values of reactant concentrations, so that it can be assumed that the influence of droplet size on nanoparticles growth is negligible.

2.13 Metal distribution in nanoparticle

Each simulation run results in a set of micelles, each one of which can contain one particle, whose composition can be different. Nanoparticle formation ends when the contents of all micelles remains constant (all metal was reduced and no more material intermicellar exchange is taking place). The composition of each micelle is monitored as a function on time, and results are averaged over 1000 runs. The final metal distribution in the nanoparticle is determined by the order with which the two metals are deposited on nanoparticle surface. To describe the structure, the sequence of metals of each nanoparticle is stored, and divided in ten concentric layers, assuming a spherical arrangement. The dispersity and averaged composition (%Au) are calculated layer by layer. The layer composition (% of each metal) is represented by a colour grading: the degradation goes from blue (0% - 10% of fast metal Au) to red (90% - 100% of Au). 50% of each metal is represented by grey. As the colour turns lighter, the proportion of pure metal in the layer is higher. The average metal distribution is showed in the histograms layer by layer: how many particles with a given percentage of Au are monitored from the inner layer (core) to the outer layer (shell). In this way, the figures show how the metal arrangement at the early stages (core) changes as the synthesis proceeds. The nanoparticle structure is also represented by means of concentric spheres, whose thickness is proportional to the number of layers with a given composition, keeping the same colour scheme.

3 Results and discussion

3.1 Reactant concentration effect on nanoparticle structure

To illustrate the dependence of nanoparticle structures on concentration when the rates ratio is moderate ($v_{Au}/v_{Pt} = 10$), the left column in Figure 1 shows the simulation results obtained keeping the film flexibility ($f = 30$, $k_{ex} = 5$) and reduction rates ratio ($v_{Au}/v_{Pt} = 10$) constant, while the metal salts concentration is increased from top to bottom (see Figures 1A, 1B and 1C). Two points can be drawn from this Figure: first, the core enrichment in Au (faster product) diminishes as concentration is increased (see red bars on the left from top to bottom). Second, the shell is enriched in Pt (slower product) with the increase of concentration (see blue bars on the right).

For a better understanding of these different behaviours, it is important to keep in mind that the synthesis of nanoparticles in microemulsions is deeply affected by the fact that the reaction media is compartmentalized.[49-55] Specifically, bimolecular electron transfer kinetics are known to be strongly affected by the compartmentalization of reactants.[55] To further investigate how compartmentalization takes part in the synthesis, the number of atoms of Au and Pt (quick and slow reduction metals) produced in all micelles during the synthesis are monitored as time goes on. From these data, the percentage of conversion of each metal is shown in the right column in Figure 1 at different initial concentrations (see Figures 1D, 1E and 1F). The red dashed line and the blue short-dashed line represent the percentage of conversion of Au and Pt respectively. The quicker obtaining of the Au, which is reduced faster, can be clearly observed. Likewise, both curves lead to a plateau when the reactants have been exhausted. As concentration increases this plateau is reached at later stages of the synthesis, as expected. The black continuous line shows the difference in the percentage of conversion between Au and Pt (%Au - %Pt) versus time at different concentrations. This difference increases as time goes on until a maximum is reached when the Au salt is almost exhausted. From this point, Pt is still appearing and the difference diminishes until it becomes insignificant when slow Pt reduction finishes. The most relevant result from this figure is the maximum displacement towards later stages together with height diminution as concentration is increased. Because this maximum reflects the highest difference in metal products availability, its temporal localization and its height will have significant consequences in the nanoparticle structure: if a remarkable maximum is located at the beginning of the synthesis, a large quantity of Au atoms are obtained when the core is forming, so the core will be essentially homogeneous and composed by Au. However, if the highest difference in metal products availability is smaller and it takes place when the metal deposition is giving rise to the middle layers, the inner ones will show a hybrid composition. This assumption can be verified by comparing both columns in Figure 1: In the upper figures, corresponding to low concentration, the maximum difference %Au - %Pt appears at the beginning (see Figure 1D), and the histogram clearly shows an Au core (see Figure 1A). Since the increase in concentration delays the %Au - %Pt maximum displacement to later stages, the cores show a progressive improvement towards a better mixture of both metals as the concentration is higher (see left column from top to bottom).

This maximum displacement to longer time can be easily understood: more collisions between droplets are needed to reach a 100% conversion of Au as concentration increases. But why the height of the maximum (largest difference %Au - %Pt) is smaller at higher concentrations is not obvious, and it is related to the reaction media compartmentalization, as explained below.

3.2 Effects of compartmentalization of reaction media on Au reduction: control by intermicellar exchange.

The results shown in previous figures were obtained using a quite flexible film, which is associated with an intermicellar exchange of 5 units of reactants (metal precursors $AuCl_4^-$ and $PtCl_6^-$, and reducing agent hydrazine) during a collision ($k_{ex} = 5$). When the initial reactant concentration is low ($\langle c_{AuCl4-} \rangle = \langle c_{PtCl6-} \rangle = 4$ metal salt per droplet), the maximum concentration gradient between two colliding droplets is 2 reactant ions, corresponding to a collision between an empty droplet and a droplet carrying 4 reactants. Since the exchange parameter k_{ex} allows a higher transfer in each collision, the material exchange rate will be limited by the concentration inside the droplets. However, at higher concentrations the reactant flow between droplets is limited by the value of the exchange parameter. For example, if one colliding droplet is empty and the other one carries 32 reactants, the crude concentration gradient principle would lead to the exchange of 16 reactants. But only $k_{ex} = 5$ reactants are allowed to be exchanged in each collision. In addition, if the exchanged reactants are $AuCl_4^-$ (faster metal precursor), reaction takes place instantaneously, and only 5 Au atoms can be obtained during each effective collision (if there is enough reducing agent). That is, the Au reduction rate is limited by the intermicellar exchange. This means that when the Au reduction rate reaches the exchange rate, it remains constant although concentration increases.

Therefore, the intuitive idea that increasing concentration will imply a rise in the Au reduction rate is not true in this compartmentalized media, as shown in Figure 2. Continuous lines in Figure 2 represent the quantity of Au produced at different concentrations as the synthesis advances. One can observe that the slope of all curves is the same, until the plateau is reached when $AuCl_4^-$ is exhausted. The only exception is for very low concentrations, where the reactant concentration appears to be the controlling factor, as expected.

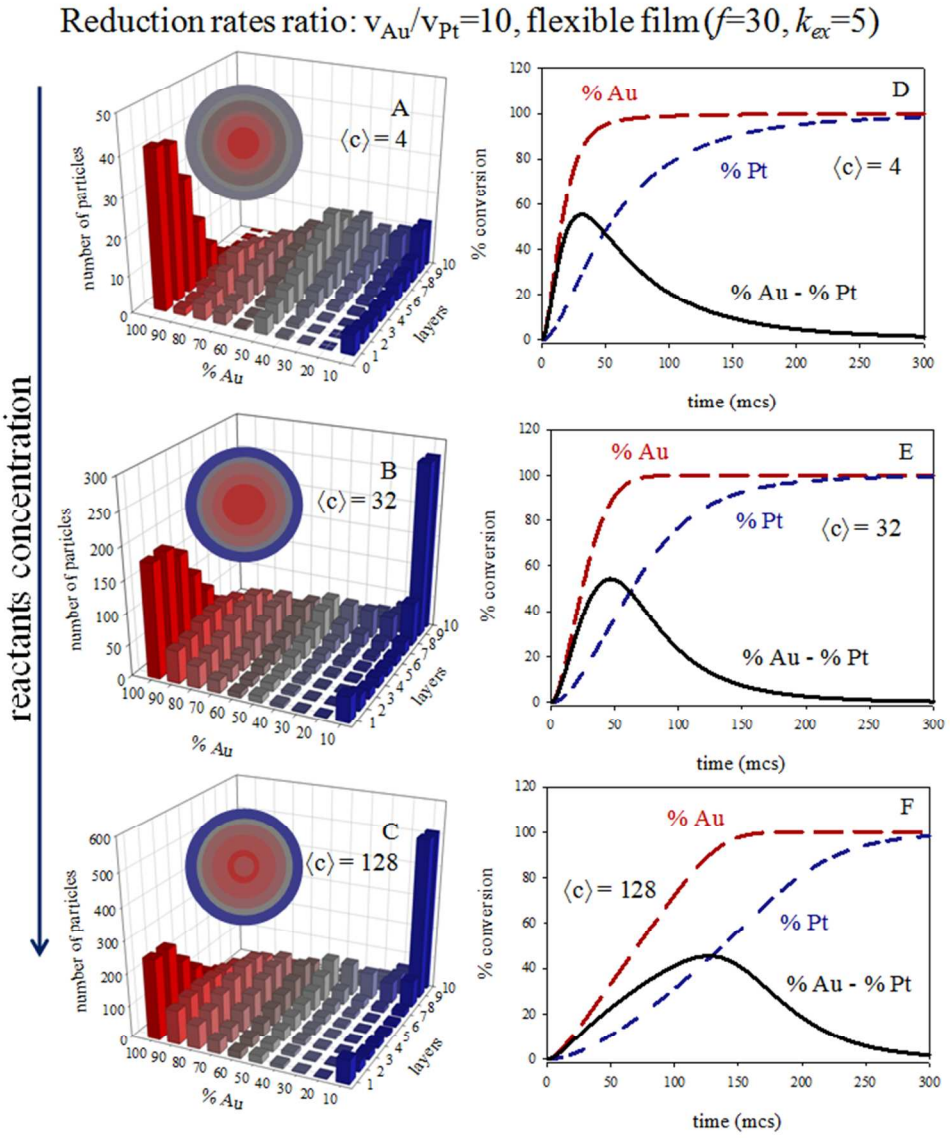

Fig. 1 Simulation results obtained keeping the reduction rate ratio (v_{Au}/v_{Pt} = 10) and the film flexibility (k_{ex} = 5, f = 30) constant and varying reactant concentration. Left column shows the number of particles versus the percentage of Au from the nanoparticle core to the outside (layer by layer). Scheme colour: blue (0% - 45% of Au), grey (45% - 55% of Au), red (55% - 100% of Au). Less red means less Au. Circles in each histogram represent nanoparticle structure in concentric layers, keeping the same colour scheme. Right column shows the percentage of Au conversion (red dashed line), the percentage of Pt conversion (blue short-dashed line), and the difference %Au - %Pt (black continuous line) versus time. A) and D) $\langle c_{AuCl4-} \rangle = \langle c_{PtCl6-} \rangle = \langle c \rangle$ 4; B) and E) $\langle c \rangle$ = 32; C) and F) $\langle c \rangle$ = 128.

3.3 Effects of compartmentalization of reaction media on Pt reduction: cage-like effect

When the exchanged reactants are slow metal precursors ($PtCl_6^-$), the restriction exchange is the same, but in addition, only a 10% of the pairs $PtCl_6^-$ and hydrazine located in the same water-pool give rise to products. The rest of reactants remain in the micelle, producing a local accumulation due to *cage-like* effect. The cage effect establishes that if a chemical reaction takes place in gas phase there will be more encounters between reactants, but they will be together a shorter time. If reaction occurs in liquid phase, there will be less encounters but they will be close together for much longer than in a gas. A similar approach can be used to compare the chemical kinetics in micelles/solution instead of liquid/gas phases. Our hypothesis is that the micelle plays the role of a cage, so each reactant encounter inside a micelle involves many collisions between reactants. That is, once $PtCl_6^-$ ions are accumulated inside a micelle, the chemical reduction continues independentally from a new intermicellar exchange. As a result, the Pt reduction rate increases due to a cage-like effect. The consequences of this phenomenon are the following: first, since the cage-like effect has only an effect on slower reduction, the differences in reduction rates of both metals

are attenuated. A more simultaneous reduction of Au and Pt will lead to a higher degree of metal mixture. Second, as the local accumulation of $PtCl_6^-$ ions is more noticeable at higher concentrations, the cage-like effect becomes more pronounced as concentration increases. This is clearly reflected in the higher slopes of the discontinuous lines (Pt reduction rate) in Figure 2. The resulting diminution in the difference of reduction rates enables us to explain the modifications in metal segregation: At the beginning of the synthesis, when the core is forming, the degree of mixture is greater if the concentration is larger (see left column in Figure 1, from top to bottom). It is important to emphasize that this more simultaneous reduction of the metals is due not only to the faster Pt reduction but also to Au reduction rate, which is limited by k_{ex} (Au cannot be reduced faster). In other words, the height of the maximum difference %Au - %Pt is lower at higher concentrations because the Au reduction rate remains constant but the Pt reduction rate increases (see right column in Figure 1).

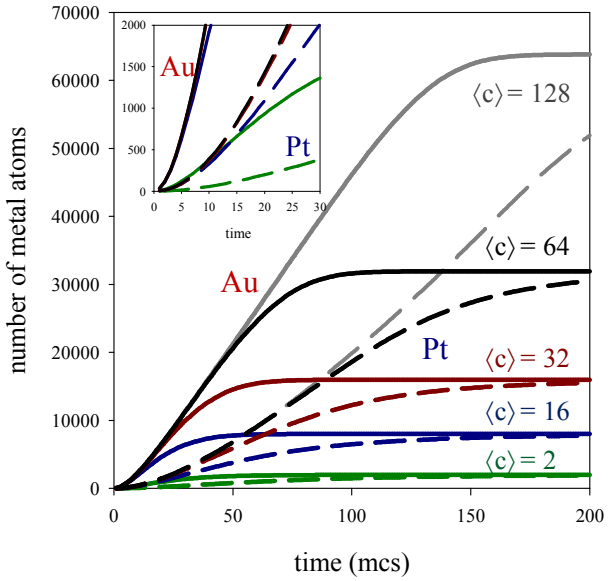

Fig. 2 Time evolution of the number of metal atoms obtained in micelles. Continuous and dicontinuous lines show the obtaining of Au and Pt respectively. Synthesis conditions: flexible film (k_{ex} = 5, f = 30), reduction rate ratio v_{Au} / v_{Pt} = 10. Green lines $\langle c_{AuCl4^-}\rangle = \langle c_{PtCl6^-}\rangle = \langle c\rangle = 2$, blue lines $\langle c\rangle$ = 16, red lines $\langle c\rangle$ = 32, black lines $\langle c\rangle$ = 64, grey lines $\langle c\rangle$ = 128 reactants per droplet.

The Pt enriched shell observed when concentration is increased can also be accounted for by the compartmentalization of reaction media. As the process advances and the maximum is exceeded, most of the Au atoms are already deposited on the particle, while the Pt atoms are still appearing. At lower concentrations, the delay in slow metal production gives rise to outer layers slightly enriched in Pt (see Figure 1A). This Pt enrichment is enhanced by higher concentration because, even though Pt acceleration favours earlier Pt deposition, high concentrations also implies that the quantity of $PtCl_6^-$ ions which remain in the reaction media from the maximum is higher. This delay in Pt obtaining causes the Pt shell formation observed at higher concentrations (see blue bars on the right in Figure 1).

In summary, compartimentalization of the reaction media plays a decisive role in Au/Pt nanoparticle formation. Due to the different behaviour of Au and Pt reduction rates when they interact with the intermicellar exchange rate, metal segregation can be modified by varying the reactants concentration.

3.4 Effects of intermicellar exchange rate on nanoparticle structure

Results clearly indicate that when a flexible film is used the nanoparticle structure can be modified by changing the concentration of the reactants. This conclusion can be generalized to different microemulsion compositions, as can be observed in the structures shown in Figure 3. This figure shows structural histograms obtained varying the film flexibility (characterized by the k_{ex} and f parameters). The structural modifications as increasing concentration are showed in Figure 3 when a rigid (see 3A, 3B and 3C), flexible (see 3D, 3E and 3F) and very flexible (see 3G, 3H and 3I) films are simulated. In the figure, surfactant film flexibility increases from left to right, and concentration increases from top to bottom. An increase in concentration leads to the progressive achievement of a more mixed core and a more Pt-enriched shell for all values of the surfactant flexibility. Likewise, if the concentration is kept constant, the degree of mixture in all layers increases as flexibility increases, as expected. This result agrees with previous simulation results on the influence of the film flexibility on metal segregation of bimetallic nanoparticles using different reduction rates[28] and different nucleation rates.[30] It is interesting to emphasize that the formation of a Pt shell can be favoured by choosing a suitable combination of exchange rate and concentration. The shell is formed when the slower reduction metal stays in the reaction medium for longer. For a fixed intermicellar exchange rate (fixed microemulsion composition), the higher the concentration, the greater the availability of Pt to form a shell at the end of the synthesis. This is clearly observed in Figure 3 (middle and right column): from top to bottom the shell is progressively more enriched in Pt. In the case of small concentration (see first file, from left to right), only nanoparticles synthesized using a rigid film show a Pt-shell: a faster reactants exchange leads to an alloyed outer layer because the higher the flexibility, the longer the ripening, and more mixed outer layers are obtained. In summary, the surface composition of Au/Pt nanoparticles can be fine-tuned by choosing the right microemulsion components and reactant concentration.

Journal Name RSCPublishing

ARTICLE

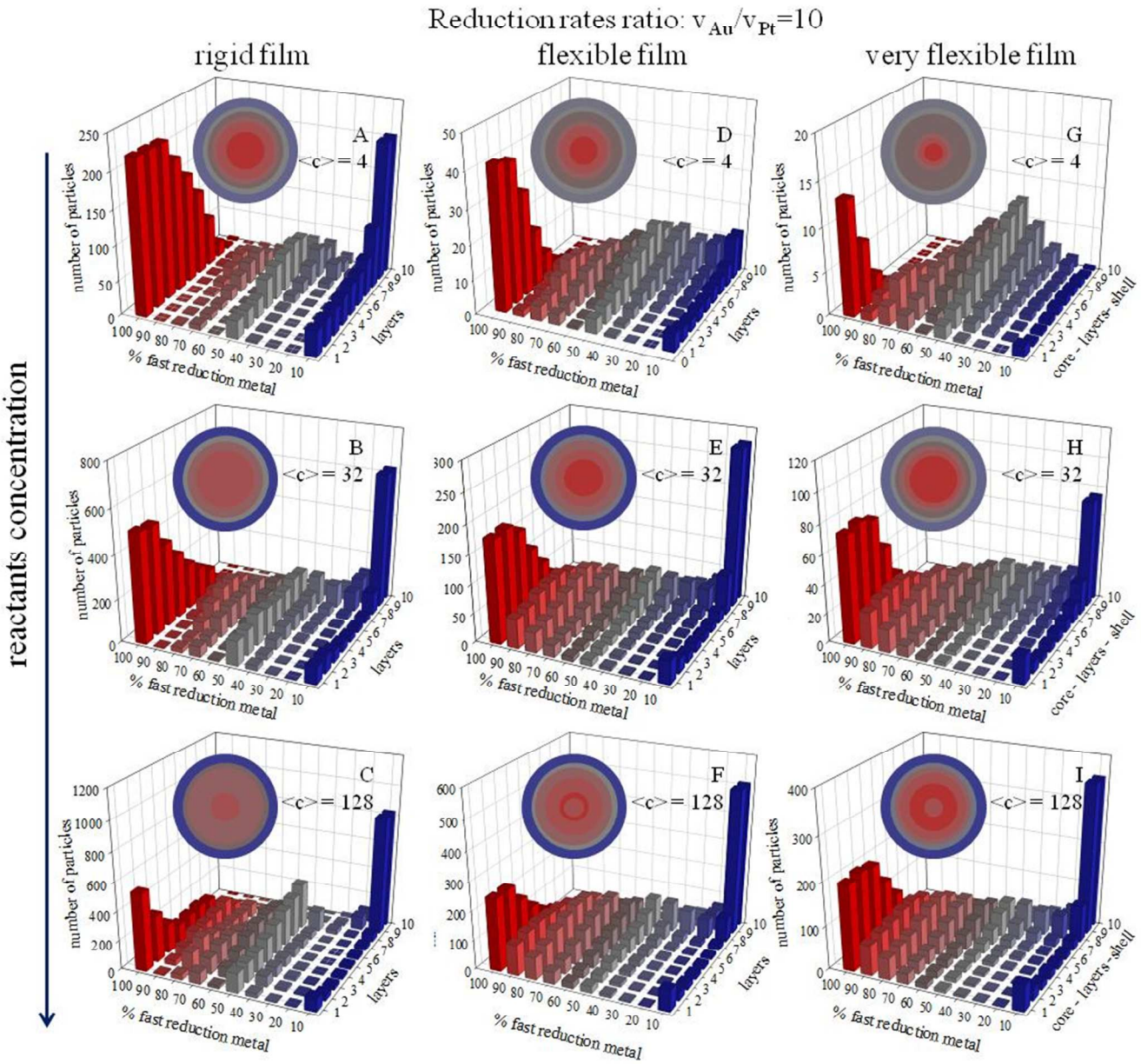

Fig. 3 Nanoparticle structures (number of particles versus the percentage of one of the metals (Au), from the nanoparticle core to the outside, layer by layer) using different values of the film flexibility and reactant concentrations. Reduction rate ratio v_{Au}/v_{Pt} = 10. Scheme colour: blue (0% - 45% of Au), grey (45% - 55% of Au), red (55% - 100% of Au). Less red means less Au. Left column: rigid film (k_{ex} = 1, f = 5); middle column, flexible film (k_{ex} = 5, f = 30); right column, very flexible film (k_{ex} = 15, f = 90). A, D and G) $\langle c_{AuCl4-} \rangle = \langle c_{PtCl6-} \rangle = \langle c \rangle$ = 4; B, E and G) $\langle c \rangle$ = 32; C, F and I) $\langle c \rangle$ = 128. Circles in each histogram represent nanoparticle structure in concentric layers, keeping the same colour scheme.

3.4 Impact of microemulsion composition on cage-like effect

In order to understand how a change in microemulsion composition affects the cage-like effect, Figure 4 shows the difference between both metal conversions vs time using different film flexibilities and concentrations. First of all, Figure 4 shows that the result obtained for a flexible film can be generalized to different flexibilities: the maximum %Au - %Pt is lower when concentration is higher due to cage-like effect. Likewise, for a fixed k_{ex}, the larger the concentration, the more displaced the maximum is, as discussed in

the previous section. Secondly, it is interesting to note that the influence of concentration is more remarkable when the film is more rigid: shorter and more displaced maxima are obtained by increasing concentration if the film is rigid, and almost overlapping maxima at all concentrations if the film is very flexible (see Figure 4C). In relation to the maximum position, it is displaced at longer stages when flexibility is decreased because more interdroplet collisions are required to reach a 100% conversion when the intermicellar exchange is slower. In relation to the height of the maximum, Figure 4 shows that, keeping concentration constant, the %Au - %Pt maximum is lower as the film is more rigid. At very low concentrations ($\langle c_{AuCl4^-} \rangle = \langle c_{PtCl6^-} \rangle = 4$), the influence of k_{ex} is almost negligible because the synthesis is controlled by concentration (compare the three continuous lines in Figure 4 A, B and C). For a better understanding of this behaviour, Figure 5 shows the time evolution of the number of atoms of Au and Pt (red continuous and blue discontinuous lines respectively) using a two different films and two different concentrations ($\langle c_{AuCl4^-} \rangle = \langle c_{PtCl6^-} \rangle = 32$ and 128). The arrows show the maximum difference %Au - %Pt in each case. It can be observed that, keeping concentration constant, both metal reduction rates are greater when a flexible film is used, because of the quicker exchange. In addition, Au and Pt curves are closer using a flexible film, due to a higher Pt accumulation (higher cage-like effect), being this effect more pronounced at higher concentrations, as could be expected. The combination of steeper slopes and closer lines gives rise to higher %Au - %Pt maximum being reached sooner using a flexible film (compare the length of the arrows). One can conclude that the cage-like effect takes place to a greater extent at higher concentrations and faster k_{ex}, giving rise to more mixed bimetallic nanostructures.

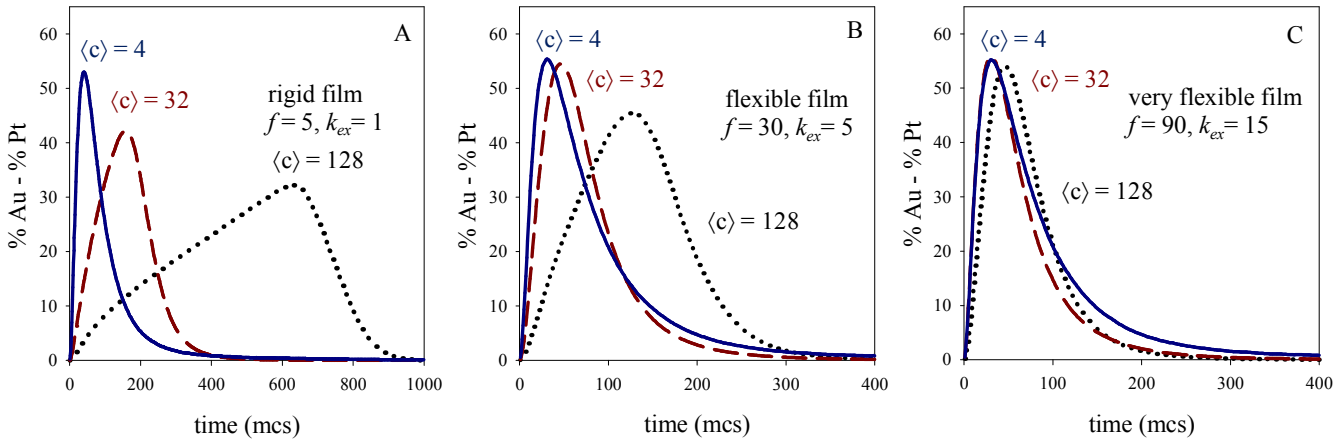

Fig. 4 Temporal evolution of the difference between Au conversion and Pt conversion, at different initial concentrations and different film flexibilities. Reduction rate ratio ($v_{Au} / v_{Pt} = 10$). A) Rigid film ($k_{ex} = 1, f = 5$). B) Flexible film ($k_{ex} = 5, f = 30$). C) Very flexible film ($k_{ex} = 15, f = 90$). Blue continuous line shows results at low concentration $\langle c_{AuCl4^-} \rangle = \langle c_{PtCl6^-} \rangle = \langle c \rangle = 4$; dashed red line corresponds to $\langle c \rangle = 32$, and dotted black line to $\langle c \rangle = 128$ reactants per droplet.

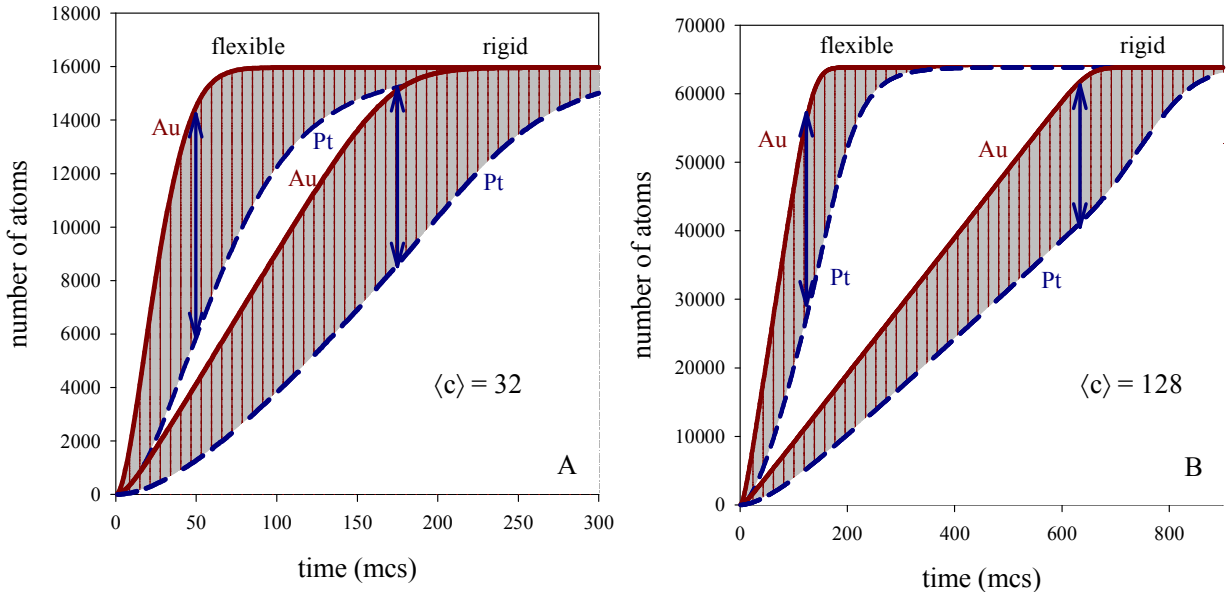

Fig. 5 Time evolution of the number of metal atoms. Red continuous and blue discontinuous lines show the obtaining of Au and Pt respectively. Synthesis conditions: flexible film ($k_{ex} = 5, f = 30$), rigid film ($k_{ex} = 1, f = 5$), reduction rate ratio $v_{Au} / v_{Pt} = 10$. A) $\langle c_{AuCl4^-} \rangle = \langle c_{PtCl6^-} \rangle = \langle c \rangle = 32$; B) $\langle c \rangle = 128$ reactants per droplet.

4. Conclusions

The compartmentalization of the reaction media causes the accumulation of slower reduced reactants in the microemulsions droplets, which favours the chemical reaction like a cage effect: The increase in local concentration of slower reduced metal gives rise to a faster reduction, and consequently, the differences in reduction rates of both metals are attenuated. A more simultaneous reduction of both metals deeply affects the nanoparticle structure, giving rise to a higher degree of mixture of both metals. This effect becomes more pronounced when the concentration is higher and intermicellar exchange is faster. For a fixed microemulsion, the nanoparticle structure can be modified by changing the reactant concentration: the core can be enriched in the faster reduction metal by lower concentrations, and the shell can be enriched in the slower metal by higher concentrations. As the design and control of spatial arrangement of Au and Pt in AuPt nanoparticles is crucial to exploiting the nanoscale bifunctional catalytic activity, our results can be used to select the best conditions to obtain a Au/Pt nanoparticle with a pre-defined structure. Conclusions can be extended to other bimetallic particles when difference in standard reduction potentials of both metals is within the 0.15 - 0.3 V range.

Abbreviations

A^+ metal precursor ($AuCl_4^-$)
B^+ metal precursor ($PtCl_6^-$)
A quicker metal (reduction product of precursor A^+): Au
B slower metal (reduction product of metal precursor B^+): Pt
R reducing agent (hydrazine)
P_i particle composed by *i* atoms of metals (A and/or B)
$\langle c_A \rangle$ mean number of the metal precursor A^+ at the beginning
$\langle c_B \rangle$ mean number of the metal precursor B^+ at the beginning
$\langle c_R \rangle$ mean number of the reductor molecules at the beginning
k_{ex} number of free units (A^+, B^+, A, B, R) which could be transferred during a collision
v_A percentage of A^+ inside the colliding droplets which gives rise to products.
v_B percentage of B^+ inside the colliding droplets which gives rise to products.
n_A* minimum number of A atoms needed to form a stable nucleus
n_B* minimum number of B atoms needed to form a stable nucleus
n_{A-B}*minimum number of A and B atoms needed to form a stable nucleus
f maximum particle size for transfer between droplets
q maximum number of metal atoms which can be carried by a droplet.

Acknowledgements

We want to acknowledge the financial support of MCI, Spain (MAT2010-20442; MAT2011-28673-C02-01), MINECO, Spain (MAT2012-36754-C02-01) and Xunta de Galicia (GRC2013-044, FEDER Funds).

Notes and references

[a] Physical Chemistry Department, Faculty of Chemistry, University of Vigo, E-36310 Vigo, Spain.

[b] Physical Chemistry Department, Faculty of Chemistry, University of Santiago de Compostela, E-15782 Santiago de Compostela, Spain.

1 M. Yashima, L. K. L. Falk, A. E. C. Palmqvist and K. Holmberg, *J. Colloid Interface Sci.,* 2003, **268**, 348-356.
2. O. P. Yadav, A. Palmqvist, N. Cruise and K. Holmberg, *Colloids Surf., A,* 2003, **221**, 131-134.
3. W. Zhang, L. Li, Y. Du, X. Wang and P. Yang, *Catal. Lett.,* 2009, **127**, 429-436).
4. S. Zhou, K. McIlwrath, G. Jackson and B. Eichhorn, *J. Am. Chem.Soc.*, 2006, **128**, 1780-1781.
5. J. Luo, P. N. Njoki, Y. Lin, D. Mott, L. Wang and C.-J. Zhong, *Langmuir*, 2006, **22**, 2892-2898.
6. H. Zhang and N. Toshima, *J. Colloid Interface Sci.*, 2013, **394**, 166-176.
7. B. N. Wanjala, J. Luo, R. Loukrakpam, B. Fang, D. Mott, P.N. Njoki, M. Engelhard, H.R. Naslund, J.K. Wu, L. Wang, O. Malis and C. J. Zhong, *Chem. Mater.*, 2010, **22**, 4282-4294.
8. H.-P. Liang, T. G. J. Jones, N. S. Lawrence, L. Jiang and J. S. Barnard, *J. Phys. Chem. C*, 2008, **112**, 4327-4332.
9. P. Hernández-Fernández, S. Rojas, P. Ocón, J. L. Gómez de la Fuente, J. San Fabián, J. Sanza, M. A. Peña, F. J. García-García, P. Terreros and J. L. G. Fierro, *J. Phys. Chem. B*, 2007, **111**, 2913-2923.
10. J. Luo, L. Wang, D. Mott, P. N. Njoki, Y. Lin, T. He, Z. Xu, B. N. Wanjala, I. I. Lim and C. J. Zhong, *Adv. Mater.*, 2008, **20**, 4342-4347.
11. J. Zhang, K. Sasaki, E. Sutter and R. R. Adzic, *Science*, 2007, **315**, 220-222.
12. J. Suntivich, Z. Xu, C. E. Carlton, J. Kim, B. Han, S. W. Lee, N. Bonnet, N. Marzari, L. F. Allard, H. A. Gasteiger, K. Hamad-Schifferli and Y. Shao-Horn, *J. Am. Chem. Soc.*, 2013, **135**, 7985-7991.
13. T. Aubert, A. Y. Ledneva, F. Grasset, K. Kimoto, N. G. Naumov, Y. Molard, N. Saito, H. Haneda and S. Cordier, *Langmuir*, 2010, **26**, 18512-18518.
14. R. Y. Parapat, V. Parwoto, M. Schwarze, B. Zhang, D.-S. Su and R. Schomäcker, *J. Mater. Chem.*, 2012, **22**, 11605-11614.
15. B. Niemann, P. Veit and K. Sundmacher, *Langmuir*, 2008, *24*, 4320-4328.
16. B. Niemann and K. Sundmacher, *J. Colloid Interface Sci.* 2010, **342**, 361-371.
17. V. Roullier, V. Marchi-Artzner, O. Cador, F. Dorson, T. Aubert, S. Cordier, Y. Molard, F. Grasset, S. Mornet and H. Haneda*, Inter. J. Nanotech.*, 2010, **7**, 46-57.
18. M. Khalid, N. Wasio, T. Chase and K. Bandyopadhyay, *Nanoscale Res. Lett.*, 2010, **5**, 61-67.
19. L. Wang, B. Qi, L. Sun, Y. Sun, C. Guo and Z. Li, *Mater. Lett.*, 2008, **62**, 1279-1282.
20. J. Luo, M. M. Maye, V. Petkov, N. N. Kariuki, L. Wang, P. Njoki, D. Mott, Y. Lin and C.-J. Zhong, *Chem. Mater.*, 2005, **17**, 3086-3091.
21. K. Holmberg, *J. Colloid Interface Sci.*, 2004, **274**, 355-364.
22. B. Wanjala, J. Luo, B. Fang, D. Mott and C. J. Zhong, *J. Mater. Chem.*, 2011, **21**, 4012-4020.
23. D. G. Angelescu, L. Magno and C. Stubenrauch, *J. Phys. Chem. C*, 2010, **114**, 22069-22078.
24. M. Wu, D. Chen and T. Huang, *Chem. Mater.*, 2001, **13**, 599-606.
25. A. Habrioux, W. Vogel, M. Guinel, L. Guetaz, K. Servat, B. Kokoh and N. Alonso-Vante, *Phys. Chem. Chem. Phys.*, 2009, **11**, 3573-3579.
26. L. M. Magno, W. Sigle, P. A. van Aken, D. Angelescu and C. Stubenrauch, *Phys. Chem. Chem. Phys.* 2011, **13**, 9134-9136.
27. C. Tojo, D. Buceta, M. Vukmirovik, R. R. Adzic and M. A. López-Quintela, *Submitted for publication*.
28. C. Tojo, M. de Dios and M. A. López-Quintela, *J. Phys. Chem. C*, 2009, **113**, 19145-19154.
29. C. Tojo and F. Barroso, *J. Colloid Interface Sci.*, 2011, **363**, 73-83.
30. F. Barroso and C. Tojo, *J. Phys. Chem. C*, 2013, **117**, 17801-17813.
31. C. Tojo, M. C. Blanco and M. A. López-Quintela, *Langmuir*, 1997, **13**, 4527-453.
32. C. Tojo, M. C. Blanco, F. Rivadulla and M. A. López-Quintela, *Langmuir*, 1997, **13**, 1970-1977.
33. P. D. I. Fletcher, A. M. Howe and B. H. Robinson, *J. Chem. Soc., Faraday Trans.*, 1987, **83**, 985-1006.
34. C. L. Kitchens, D. P. Bossev and C. B. Roberts, *J. Phys. Chem. B*, 2006, **110**, 20392-20400.
35. M. R. Housaindokht and A. N. Pour, *Solid State Sci.*, 2012, **14**, 622-625.
36. V. K. La Mer and R. H. Dinegar, *J. Am. Chem. Soc.*, 1950, **72**, 4847-4854.
37. B. Niemann and K. Sundmacher, *Chem. Engineering J.*, 2008, **143**, 314-325.

38. A. Ritcey, J. Lemyre, A. Beaupré and S. Lamarre, *Langmuir*, 2011, **27**, 11824-11834.
39. F. Barroso, M. de Dios, C. Tojo, M. C. Blanco and M. A. López-Quintela, *Colloids Surf., A*, 2005, **270**, 78-82.
40. B. Niemann, F. Rauscher, D. Adityawarman, A. Voigt and K. Sundmacher, *Chem. Engineering Proc.*, 2006, **45**, 917-935.
41. L. Deng, W. Hu, H. Deng and S. Xiao, *J. Phys. Chem. C*, 2010, **114**, 11026-11032.
42. S. Xiong, W. Qi, B. Huang and M. Wang, *Chem. Phys. Chem*., 2011, **12**, 1317-1324.
43. S. Quintillán, C. Tojo, M. C. Blanco and M.A. López-Quintela, *Langmuir*, 2001, **17**, 7251-7254.
44. R. Jain and A. Mehra, *Langmuir*, 2004, **20**, 6507-6513.
45. A. R. Kumar, G. Hota, A. Mehra and K. Khilar, *AIChE J.*, 2004, **50**, 1556-1567.
46. D. Andelman, M. E. Cates, D. Roux and S. A. Safran, *J. Chem. Phys*., 1987, **87**, 7229-7241.
47. M. E. Cates, D. Andelman, S. A. Safran and D. Roux, *Langmuir*, 1988, **4**, 802-806.
48. M. A. López-Quintela, J. Rivas, M. C. Blanco and C. Tojo, in *Nanoscale Materials*, Eds. L. M. Liz-Marzán, Kluwer Academic Publishers, Boston, 2003, p. 135-155.
49. M. A. López-Quintela, C. Tojo, M. C. Blanco, L. García Río and J. R. Leis, *Curr. Opin. Colloid Interface Sci.*, 2004, **9**, 264-279.
50. M. P. Pileni, *J. Phys. Chem*., 1993, **97**, 6961-6973.
51. J. Eastoe, M. J. Hollamby and L. Hudson, *Adv. Colloid Interface Sci.*, 2006, **128-130**, 5-15.
52. M. P. Pileni, *Nature Mater.*, 2003, **2**, 145-150.
53. A. E. C. Palmqvist, *Curr. Opin. Colloid Interface Sci.*, 2003, **8**, 145-155.
54. N. Weitbrecht, M. Kratzat, S. Santoso, R. Schömacker, *Catal. Today*, 2003, 79-80, 401-408.
55. S. D. Choudhury, M. Kumbhakar, S. Nath, S. K. Sarkar, T. Mukherjee and H. Pal, *J. Phys. Chem. C*, 2007, **111**, 8842-8853.